E_T and other Event-by-Event Distributions from AGS to RHIC energies.

M. J. Tannenbaum[1]

[1] Brookhaven National Laboratory, Upton, NY 11973-5000 USA

November 20, 2003

Abstract

Event-by-event distributions in multiplicity, E_T and $\langle p_T \rangle$ are illustrated and techniques to understand them are discussed.

1 Multiplicity in collisions of nucleons and nuclei

Many modern multiplicity measurements do not simply count the all particles produced on each interaction, but, rather, measure single particle and multi-particle "inclusive" cross-sections. A single particle inclusive reaction involves the measurement of just one particle coming out of a reaction,

$$a + b \rightarrow c + \text{anything} \quad .$$

The terminology comes from the fact that all final states with the particle c are summed over, or **included**. A "semi-inclusive" reaction refers to the measurement of all events of a given topology or class, e.g.

$$a + b \rightarrow n_1 \text{ particles of class } 1 + \text{anything} \quad ,$$

where "centrality" is the most common class in relativistic heavy ion collisions.

Measurements are presented in terms of the (Lorentz) Invariant single particle inclusive differential cross section (or Yield per event in the class if semi-inclusive):

$$\frac{Ed^3\sigma}{dp^3} = \frac{d^3\sigma}{p_T dp_T dy d\phi} = \frac{1}{2\pi}\,\mathbf{f}(p_T, y) \quad , \tag{1}$$

where y is the rapidity, p_T is the transverse momentum, and ϕ is the azimuth of the particle. It is important to be aware that the integral of the single particle inclusive cross section over all the variables is not equal to σ_I the interaction cross section, but rather is equal to the mean multiplicity times the interaction cross section : $< n > \times \sigma_I$. Hence the mean multiplicity per interaction is

$$\langle n \rangle = \frac{1}{\sigma_I} \int \frac{d\phi}{2\pi} dy\, dp_T\; p_T\; \mathbf{f}(p_T, y) = \frac{1}{\sigma_I} \int dy\, \frac{d\sigma}{dy} = \int dy\, \frac{dn}{dy} = \int dy\, \rho(y) \quad , \tag{2}$$

where the terminology for the multiplicity density in rapidity is $\rho(y) = dn/dy$ for identified particles (m known), $dn/d\eta$ for non-identified particles (m unknown, assumed massless), where $\eta = -\ln\tan(\theta/2)$ is the pseudo-rapidity.

Measurements of $dn/d\eta$ in pp, $\bar{p}p$ collisions from c.m. energy $\sqrt{s} = 53$ to 900 GeV [1] are shown in Fig. 1 in the left most panel. This multiplicity is normalized to σ_{NSD}, the non-single diffractive cross section; clearly the multiplicity per inelastic collision would be smaller. Although not explicitly stated

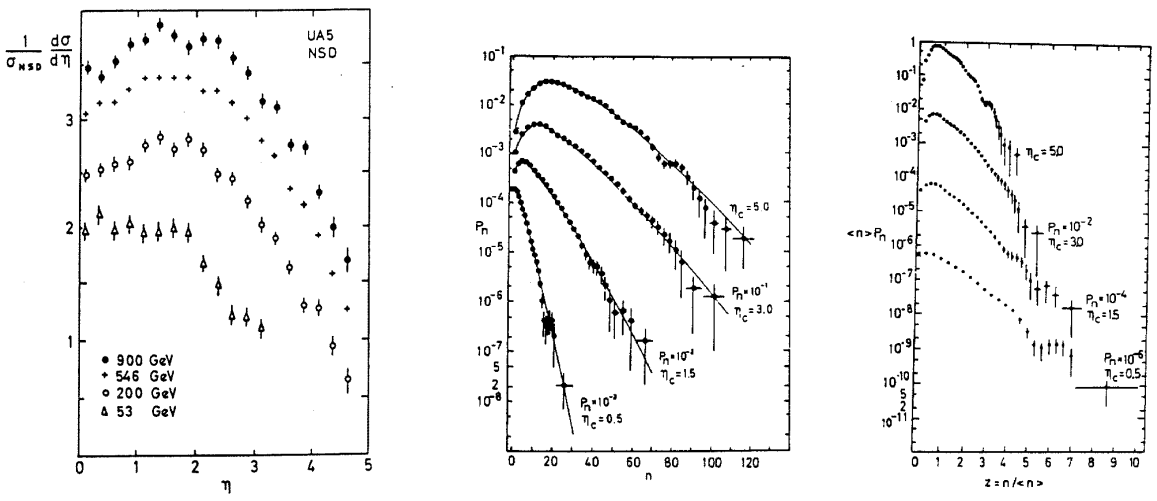

Figure 1: Charged multiplicity measurements from UA5[1, 2].

so far, $dn/d\eta$ is an average over all events. UA5 found (center and right panels) that the event-by-event distribution of multiplicity in small regions of $\Delta\eta$ was much more interesting than the average multiplicity [2]. The center panel is the relative frequency distribution of the multiplicity n in an interval of pseudo-rapidity $|\eta| < \eta_c$ for each event in a large sample. The study of distributions in small intervals near mid rapidity should allow observation of the "real" multiplicity fluctuations, freed of the constraints of energy, momentum and charge conservation, which need not be locally conserved. UA5 found that the multiplicity distributions were Negative Binomial, not Poisson, which implies correlations [2]. In the right panel, where the multiplicity distribution in interval η_c is scaled by the mean in that interval, the distributions clearly show larger fluctuations, the smaller the interval—they do not "scale in the mean".

2 E_T (or Transverse Energy) Distributions

E_T is an event-by-event variable defined as:

$$E_T = \sum_i E_i \sin\theta_i \qquad \text{and} \qquad dE_T(\eta)/d\eta = \sin\theta(\eta)\, dE(\eta)/d\eta \qquad , \tag{3}$$

The sum is taken over all particles emitted on an event into a fixed but large solid angle, (which is different in every experiment). E_T distributions are measured in both Hadronic and Electromagnetic Calorimeters and even as a sum of charged particles $\sum_i |p_{T_i}| \equiv E_{Tc}$. E_T was introduced by High Energy Physicists [3] as an "improved" method to detect and study the jets from "hard-scattering" compared to high p_T single particle spectra by which hard scattering was discovered in pp collisions (and used as a hard-probe in Au+Au collisions at RHIC [4]). However, this idea didn't work as expected: E_T distributions are dominated by soft particles near the $\langle p_T \rangle$.

The first measured E_T distribution in the present day usage of the terminology is by the NA5 experiment [5] in pp collisions (Fig. 2-left). The detector was essentially the same hadron calorimeter (ring calorimeter) as used in the NA35 heavy ion experiment[6], covering the full azimuth and c.m. pseudo-rapidity interval $-0.88 < \eta^* < 0.67$ at pp c.m. energy $\sqrt{s} = 23.7$ GeV. When these data

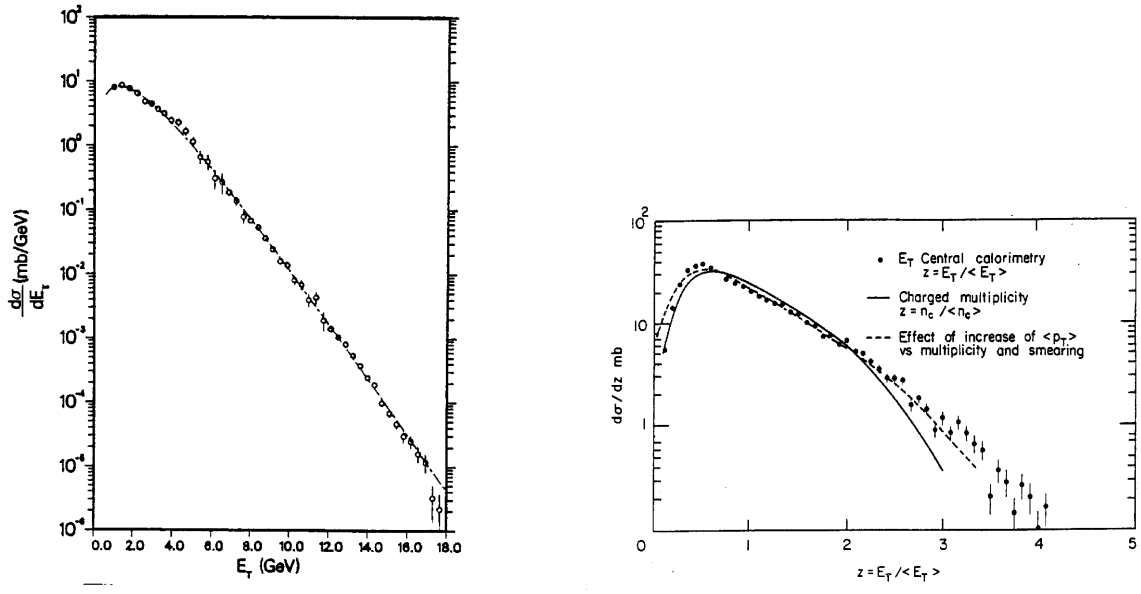

Figure 2: (left) E_T distribution from NA5 [5];(right) E_T and charged multiplicity distributions from UA1 [7].

were first presented in 1980, they shocked the world of high energy physics because they provided no evidence for jets. The situation was not resolved until the International High Energy Physics conference of 1982 when two important results were presented from the CERN $\bar{p}p$ Collider at $\sqrt{s} = 540$ GeV. The UA1 collaboration [7] measured both the E_T distribution in their central calorimeter and the charged multiplicity distribution in their central tracker and found that they were the same shape when scaled by the mean of each quantity (Fig. 2-right). This important result established that E_T is like multiplicity: composed of many soft particles near the $\langle p_T \rangle$. However, this result was overshadowed by the first detection of a jet by UA2 [8], 5 orders of magnitude down in their E_T distribution. These two results firmly established that the jet contribution to E_T distributions is negligible and that E_T is essentially an analog method of measuring the multiplicity of particles produced on an event: the E_T distribution is the random product of the multiplicity and transverse momentum distributions of the particles—$dE_T/dy \sim < p_T > \times dn/dy$.

3 E_T distributions in RHI Collisions

The importance of E_T distributions in relativistic heavy ion (RHI) collisions is that they are largely dominated by the *nuclear geometry* of the reaction and so provide a measure of the overall character or *centrality* of individual RHI interactions. According to Bjorken[9], the transverse energy flow in rapidity, dE_T/dy, is thought to be related to the co-moving energy density in a longitudinal expansion, and proportional to the energy density in space ϵ:

$$\epsilon_{Bj} = \frac{1}{\tau_0 \, \pi R^2} \frac{d < E >}{dy} = \frac{1}{\tau_0 \, \pi R^2} \frac{dE_T}{dy} \tag{4}$$

where τ_0, the formation time, is usually taken as 1 fm, πR^2 is the effective area of the collision, and $d < E > /dy$ is the co-moving (i.e. transverse) energy density.

The first measurement of an E_T distribution in Relativistic Heavy Ion collisions was by the NA35 Collaboration [6] at the CERN fixed target program in ^{16}O+Pb collisions at mid-rapidity for $\sqrt{s_{NN}} =$ 19.4 GeV using the same hadron calorimeter as NA5 [5]. Fig. 3 shows the E_T distributions in p+Au (left)

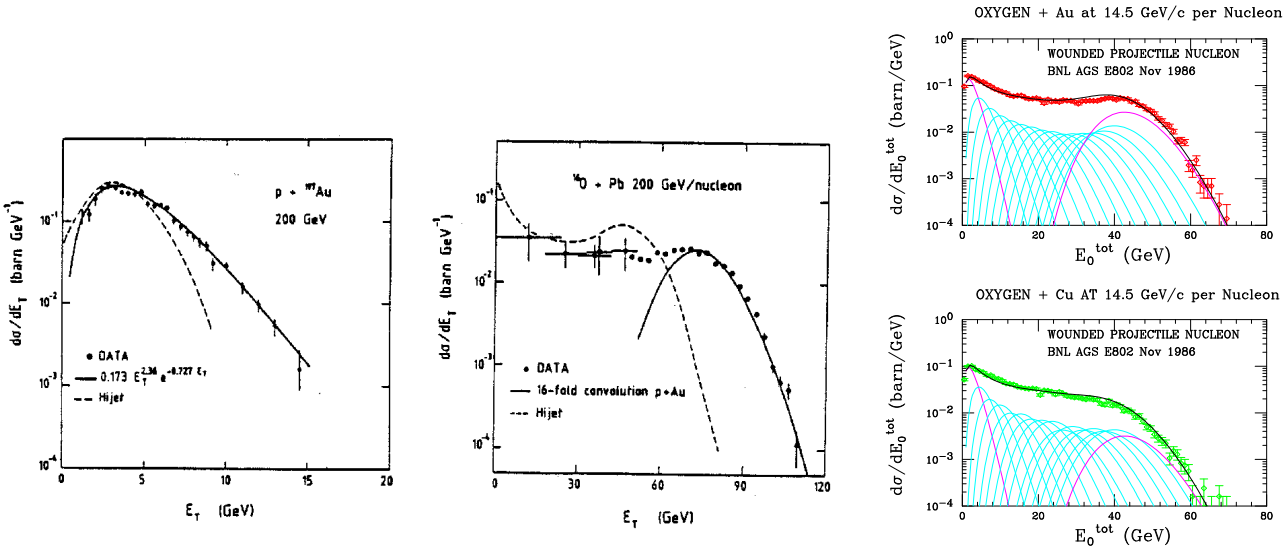

Figure 3: E_T distributions: (left,center) NA35 [6]; (right) E802 [10].

and ^{16}O+Pb (center) from which NA35 concluded that the upper edge of the O+Pb E_T distribution is given by the 16-fold convolution of the p+Au distribution. This is called the Wounded Projectile Nucleon Model (WPNM). This result was followed very quickly by a result from E802 [10] (Fig 3-right), which showed that the WPNM worked in detail: the *full* O+Cu and O+Au E_T distributions could be described by the 1–16 fold convolution of the measured p+Au E_T distribution, weighted by the probability of the 1–16 projectile nucleons to interact at least once in the target. Note that the maximum energy in O+Cu is the same as in O+Au and that the upper edge of both spectra are virtually identical above 50 GeV if the Cu cross section is multiplied by a factor of ~ 6. This was the first indication of large stopping at the AGS: the ^{16}O projectiles are sufficiently stopped in Cu so that energy emission at mid-rapidity effectively ceases.

3.1 The shapes of E_T distribution

Figs. 2-left, 3-left, and 3-center, show the evolution of the shape of the E_T distributions in the same detector from pp to p+A to A+A collisions. In both pp and p+Au collisions the shape of the E_T distribution for NA35 is given by a simple Gamma distribution illustrated by the solid lines on the figures ($p = 2.4$ in pp, 3.4 in p+Au). However the ^{16}O+Au spectrum (Fig. 3-right) shows the now "classical" $A - A$ spectral shape: an initial fall-off and then a broad plateau, a peak at the end of the plateau where the curve turns over (the 'knee') and then a sharp exponential drop-off until the sensitivity runs out. The light lines on Fig. 3-right are 1–16-fold convolutions of the measured p+Au spectral shape in the E802 detector (a Gamma distribution with $p = 2.6 \pm 0.2$).

3.1.1 Statistical independence and convolutions

In mathematical statistics, convolutions arise from the sums of mutually independent random variables. The probability distribution of a random variable S_n, which is itself the sum of n **independent** random variables with a common distribution $f(x)$:

$$S_n = x_1 + x_2 + \cdots + x_n \tag{5}$$

is given by $f_n(x)$, the n-fold convolution of the distribution $f(x)$:

$$f_n(x) = \int_0^x dy\, f(y)\, f_{n-1}(x-y) \qquad . \tag{6}$$

The mean, $\mu_n = \langle S_n \rangle$, and standard deviation, σ_n, of the n-fold convolution obey the familiar rule

$$\mu_n = n\mu \qquad \sigma_n = \sigma\sqrt{n} \quad , \tag{7}$$

where μ and σ are the mean and standard deviation of the distribution $f(x)$.

3.1.2 The Gamma distribution

Just as the Negative Binomial Disrtibution (NBD) fits the charged particle multiplicity distribution in pp collisions, the Gamma distribution fits the E_T distributions. Moreover, the Gamma distribution is an example of a probability density function (pdf) which has particularly simple properties under convolutions and scale transformations (so does the NBD, but no space for discussion here). The Gamma distribution is a function of a continuous variable x and has paramters p and b

$$f(x) = f_\Gamma(x, p, b) = \frac{b}{\Gamma(p)}(bx)^{p-1}e^{-bx} \tag{8}$$

where

$$p > 0, \quad b > 0, \quad 0 \leq x \leq \infty$$

$\Gamma(p) = (p-1)!$ if p is an integer, and $f(x)$ is normalized, $\int_0^\infty f(x)dx = 1$. The mean and standard deviation of the distribution are

$$\mu \equiv \langle x \rangle = \frac{p}{b} \qquad \sigma \equiv \sqrt{\langle x^2 \rangle - \langle x \rangle^2} = \frac{\sqrt{p}}{b} \qquad \frac{\sigma^2}{\mu^2} = \frac{1}{p} \qquad . \tag{9}$$

The n-fold convolution of the Gamma distribution (Eq. 8) is simply given by the function

$$f_n(x) = \frac{b}{\Gamma(np)}(bx)^{np-1}e^{-bx} = f_\Gamma(x, np, b) \tag{10}$$

i.e. $p \to np$ and b remains unchanged. Note that the mean and standard deviation of Eq. 10

$$\mu_n = \frac{np}{b} \qquad \sigma_n = \frac{\sqrt{np}}{b} \qquad \frac{\sigma_n}{\mu_n} = \frac{1}{\sqrt{np}} \tag{11}$$

when compared to Eq. 9 explicitly obey Eq. 7. To summarize, the n-th convolution of the Gamma distribution $f_\Gamma(x, p, b)$ is $f_\Gamma(x, np, b)$—b remains unchanged.

3.2 Extreme-Independent Models

The WPNM is an example of an extreme-independent model, where particle production takes place entirely outside the volume of the colliding nuclei, so that there is no cascading. Thus, extreme-independent models separate the overlap geometry of the nuclear collision from the dynamics of particle production. The Nuclear Geometry is represented as the relative probability, w_n, on a B+A interaction for a given number of projectile participants (WPNM), total participants (Wounded Nucleon Model—WNM) [11], wounded projectile quarks (Additive Quark Model) [12] or other fundamental element of particle production. The dynamics of particle production, the distribution of particles or E_T for the fundamental element, is taken from the data. For instance, the measured E_T distribution for a pp collision represents 2 participants, 1 NN binary-collision, 1 wounded projectile nucleon, or a predictable convolution of quark-nucleon collisions.

The WPNM calculation for a B+A reaction is given by the sum:

$$\left(\frac{d\sigma}{dE_T}\right)_{\rm WPNM} = \sigma_{BA} \sum_{n=1}^{B} w_n \, P_n(E_T) \tag{12}$$

where σ_{BA} is the measured B+A cross section in the detector aperture, w_n is the relative probability for n projectile nucleons in the B+A reaction and $P_n(E_T)$ is the calculated E_T distribution on the detector aperture for n **independently interacting** projectile nucleons. If $f_1(E_T)$ is the measured E_T spectrum on the detector aperture for one projectile nucleon, and p_0 is the probability for the elementary collision to produce no signal on the detector aperture, then, the correctly normalized E_T distribution for one projectile nucleon collision is:

$$P_1(E_T) = (1 - p_0) f_1(E_T) + p_0 \delta(E_T) \qquad , \tag{13}$$

where $\delta(E_T)$ is the Dirac delta function and $\int f_1(E_T)\, dE_T = 1$. $P_n(E_T)$ (including the p_0 effect) is obtained by convoluting $P_1(E_T)$ with itself $n-1$ times

$$P_n(E_T) = \sum_{i=0}^{n} \frac{n!}{(n-i)!\; i!}\, p_0^{n-i} (1-p_0)^i f_i(E_T) \tag{14}$$

where $f_0(E_T) \equiv \delta(E_T)$ and $f_i(E_T)$ is the i-th convolution of $f_1(E_T)$.

3.2.1 The number of projectile participants can be measured

The number of projectile participants is not a purely abstract quantity, it can be measured, typically by a Zero Degree Calorimeter which, in fixed target collisions, detects the projectile spectators remaining at beam rapidity after the collision. The projectile participants for a given event are just the total number of nucleons in the projectile minus the measured spectators. Fig. 4-left shows a measurement by the WA80 collaboration [13] at CERN of $E_{\rm ZDC}$ the energy of spectators versus the average mid-rapidity

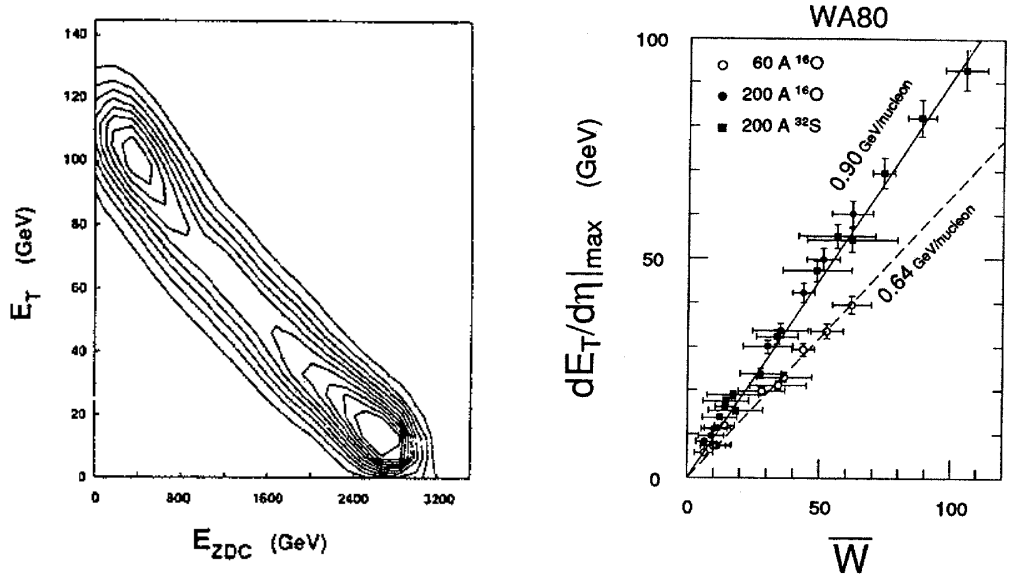

Figure 4: Measurements from WA80 [13]:(left) E_T vs $E_{\rm ZDC}$; (right) test of WNM.

E_T observed for 200 A·GeV ^{16}O+Au collisions. As the impact parameter reduces from grazing impact, more nucleons participate (there are fewer spectators) so more energy is transferred from the projectile and target rapidity regions to the transverse direction and toward mid-rapidity, resulting in increased E_T. WA80 also checked the WNM in detail by measuring the mid-rapidity $dE_T/d\eta$ as a function of $\overline{\rm W} = \langle N_{part} \rangle$, the average number of participants, at two incident energies and for ^{16}O and ^{32}S on Au—The linear relationship shows that the WNM works at CERN fixed target energies [14].

3.3 Systematics of E_T distribution at various $\sqrt{s_{NN}}$

Actually, the only place where the WNM works is at CERN/FNAL Fixed Target energies, $\sqrt{s_{NN}} \sim 20$ GeV. The WNM underpredicts for higher c.m. energies, $\sqrt{s_{NN}} \geq 31$ GeV, and overpredicts at AGS energies, $\sqrt{s_{NN}} \sim 5$ GeV, where the WPNM works at mid-rapidity.

E_T distributions for pp dd and $\alpha - \alpha$ collisions at $\sqrt{s_{NN}} = 31$ GeV at the CERN ISR [15] are shown in Fig. 5-left. Fig. 5-center shows: a Gamma distribution fit with $p = 2.50 \pm 0.06$ for the pp data; a

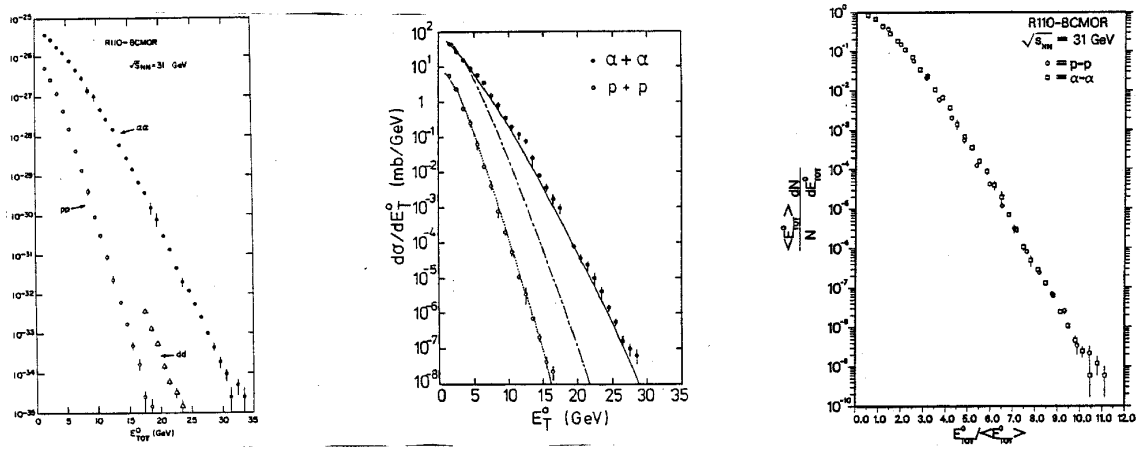

Figure 5: R110-BCMOR E_T distributions at $\sqrt{s_{NN}} = 31$ GeV [15, 16].

WNM calculation for the $\alpha - \alpha$ data (dot-dash line) using the pp fit, which does describe the data for the first order of magnitude, but totally misses the upper tail; and an AQM calculation [16], which fits the $\alpha - \alpha$ data. Interestingly, a single Gamma distribution with the same $p = 2.48 \pm 0.05$ as the pp data fits the $\alpha - \alpha$ data, which implies that the pp and $\alpha - \alpha$ data have virtually identical shapes over 10 decades when scaled by their respective means Fig. 5-right. We still don't know whether this is a fluke or important Physics.

The situation at AGS energies, $\sqrt{s_{NN}} \sim 5$ GeV is still different (see Fig. 6) [17]. The 8 panels on the left show the mid-rapidity E_T distributions for p+Au and p+Be as a function of $\delta\eta$ interval. The p+Au and p+Be have identical Gamma distribution shapes to each other (parameters given on plot) which change in lockstep over a wide range in $\delta\eta$—the WNM utterly fails![1] In the 4 panels on the right are the p+Au, O+Cu, Si+Au and Au+Au E_T distributions as a function of $\delta\eta$, where the lines are WPNM calculations based on the p+Au fit in each interval—reasonable, but not perfect agreement.

The E802 data in Fig. 6 have no correction for the EMcalorimeter response or for the solid angle. The measurement in any solid angle is very precise but is not accurate, clearly good for A dependences in a single setup, but not as good (larger systematic errors) for comparison of different experiments. Two improved ways of presenting the Au+Au data are illustrated in Fig. 7: (left) E_T in the measured aperture is corrected to E_T in $\Delta\Phi = 2\pi$ $\Delta\eta = 1$ for all 4 $\delta\eta$ intervals without (or ideally, with) HAD/EM calorimeter response correction; (right) E_T scale is corrected to $E_T/\langle E_T \rangle_{pp}$, i.e. E_T in units of $\langle E_T \rangle$ per participant pair, using the measured $\langle E_T \rangle_{pp}$ for pp collisions in same aperture. The larger fluctuations for smaller apertures are now clearly visible. In actual fact, the plot in Fig. 7-right, was scaled by the measured $\langle E_T \rangle_{\mathrm{p+Au}}$, but it gives the correct measurement "per participant pair", since the WPNM applies rather than the WNM. This can be seen in Fig. 8-left, where the distribution from the largest interval, $1.22 \leq \eta \leq 2.50$, from Fig. 7-right is compared directly to the probability distribution for $N_{\mathrm{part}}/2$. The E_T distribution follows the nuclear geometry very accurately until roughly the top 4-percentile of the distribution, where the underlying fluctuations begin to show once the nuclear geometry

[1] This confirms the original AGS stopping measurement [18] and the explanation that the pion distribution for the second collision shifts by > 0.8 units in η, i.e. well away from mid-rapidity.

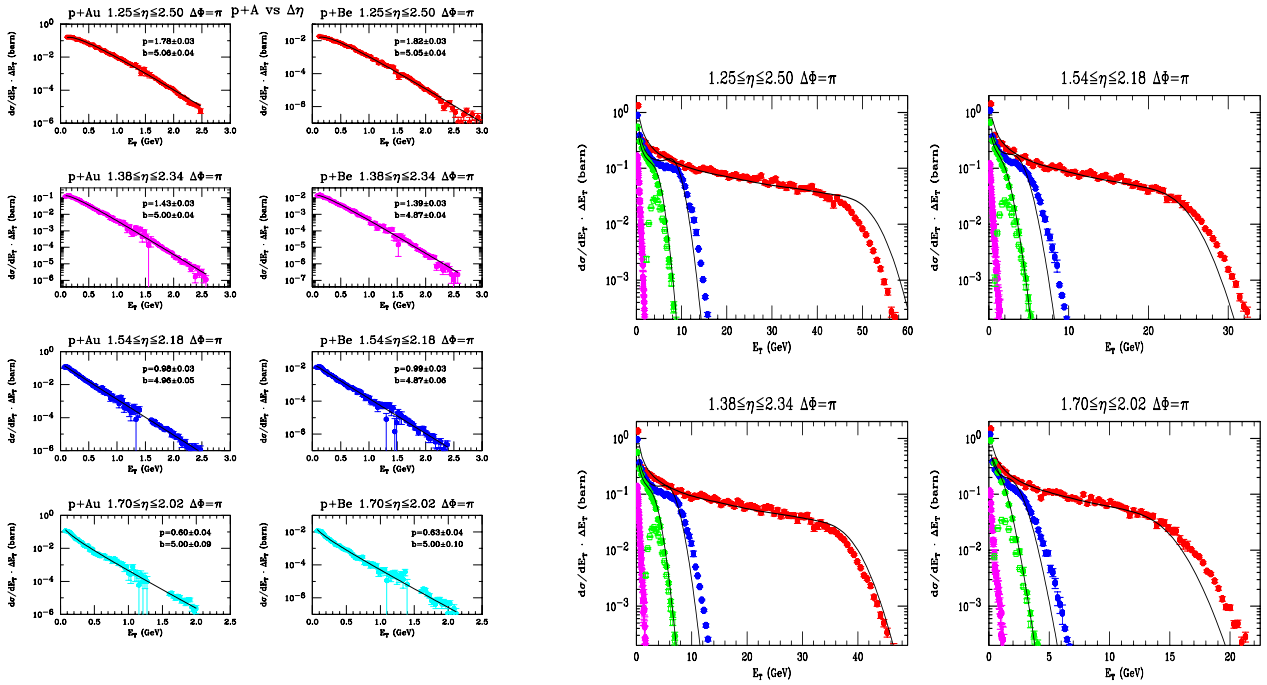

Figure 6: E_T distributions vs $\delta\eta$ from AGS-E802 [17].

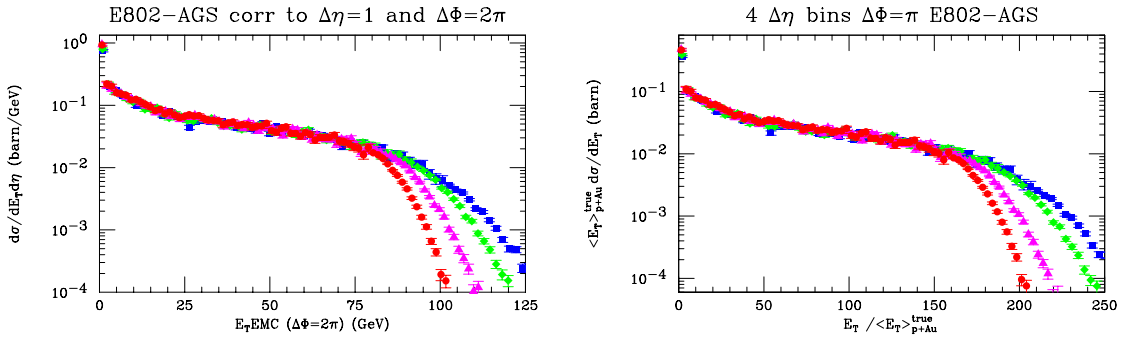

Figure 7: The Au+Au E_T distributions from Fig. 6, scale corrected in two different ways.

is exhausted. This is illustrated by the WPNM calculation in Fig. 8-right, where the individual n-fold convolutions of the fundamental distribution are shown.

3.4 Results from RHIC

The $E_T(\Delta\Phi = 2\pi\ \Delta\eta = 1)$ distributions from PHENIX at RHIC [20] for Au+Au collisions at $\sqrt{s_{NN}} =$ 200 GeV for 5 $\delta\phi$ intervals of $1, 2, \ldots 5 \times 22.4°$ are shown in Fig. 9-left, compared to the E802 E_T distribution from Fig. 7-left. At RHIC, about 2-3 times more E_T and multiplicity than predicted by the WNM are observed [20, 21]. It is interesting to compare the shapes of the Au+Au E_T distributions at AGS and RHIC by simply scaling the AGS-E802 distribution by an empirical factor of 8.1 (Fig. 9-right)—the distributions are exactly the same shape, even though the underlying production dynamics are totally different. This is yet to be understood.

Fig. 9 also indicates larger fluctuations of E_T with decreasing solid angle. In order to answer the question of whether these fluctuations are random or due to correlations, we look at the event-by-event

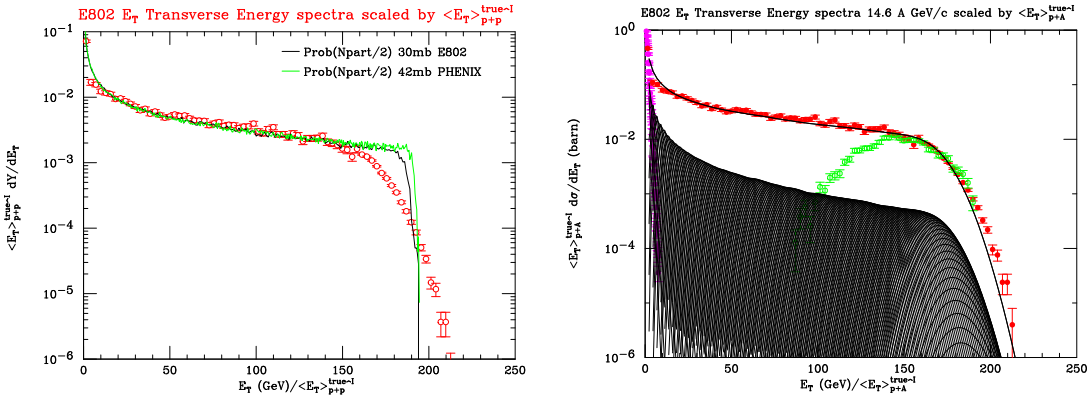

Figure 8: E802 distribution in $E_T/\langle E_T\rangle_{\rm p+Au}$ compared to w_n (left), WPNM calculation(right)

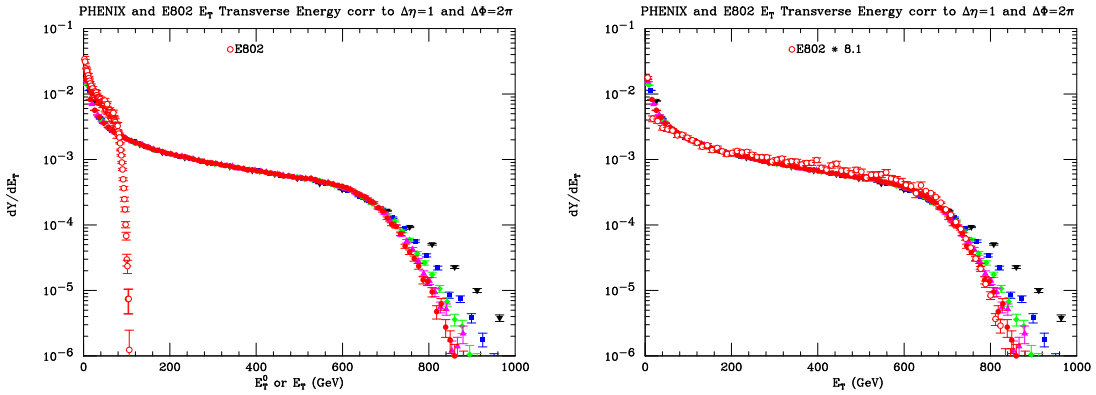

Figure 9: PHENIX E_T distributions [20] for Au+Au at RHIC compared to E802 at AGS: (left) E802 absolute scale from Fig. 7-left; (right) E802 data scaled by 8.1 to compare shape.

distribution of the average p_T of charged particles [22]:

$$M_{p_T} = \overline{p_T}_{(n)} = \frac{1}{n}\sum_{i=1}^{n} p_{T_i} = \frac{1}{n} E_{Tc} \qquad . \tag{15}$$

The event-by-event average Eq. 15 is closely related to the event-by-event sum Eq. 3, and also follows Gamma distributions [19]. Fig. 10-left, shows the event-by-event distribution of M_{p_T} as data points, with mixed events (histogram) representing a random sample. Barely visible to the naked eye, the standard distribution of the data is slightly larger than the random sample as represented by $F_{p_T} \equiv \sigma_{M_{p_T}}/\sigma_{random} - 1$ (Fig. 10-center, Fig. 10-right). F_{p_T} first increases with the centrality (N_{part}) and then decreases. F_{p_T} from pp collisions ($N_{part} = 2$) is also shown. F_{p_T} also increases with the maximum p_T of tracks used in the average (Fig. 10-right). These small correlations of a few percent are explained as due to jets [22], which is quite different than the observations at lower $\sqrt{s_{NN}}$ [23].

The absence or small size of soft-fluctuations at RHIC remains a mystery.

References

[1] UA5 Collab., K. Alpgard *et al., Phys. Lett.* B 123 (1983) 361

[2] UA5 collaboration, G. J. Alner, *et al., Phys. Lett.* B 160 (1985) 193 ; see also UA5 collaboration, G. J. Alner, *et al., Phys. Rep.* 154 (1987) 247 , and references therein.

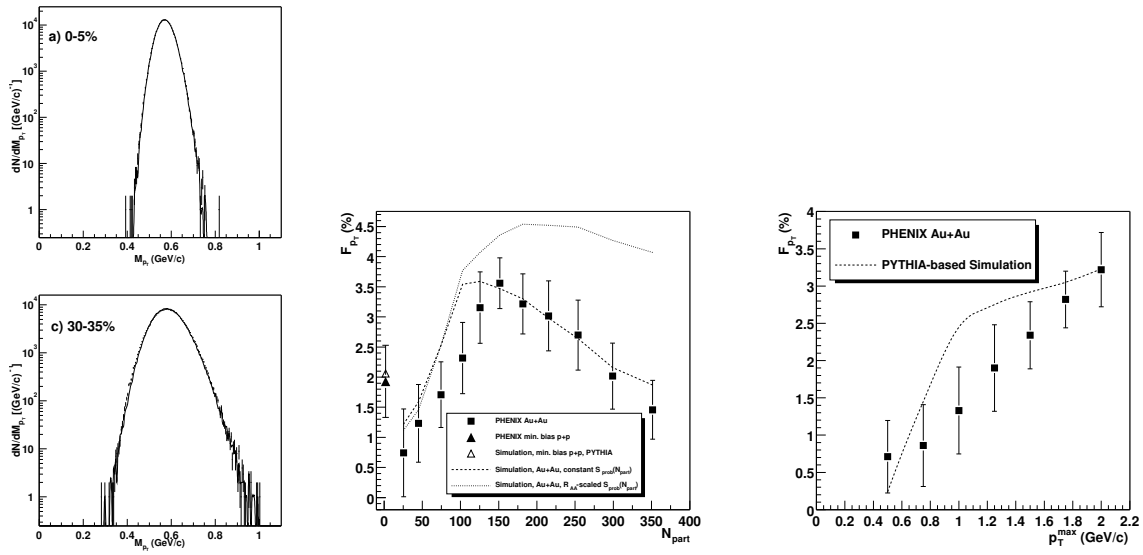

Figure 10: PHENIX measurements [22] of M_{p_T} (left); and F_{p_T} (center,right).

[3] See, for example, M. J. Tannenbaum, *Int. J. Mod. Phys.* A 4 (1989) 3377 , and references therein.

[4] PHENIX Collaboration, K. Adcox, *et al.*, *Phys. Rev. Lett.* 88 (2002) 022301

[5] C. DeMarzo *et al.,* *Phys. Lett.* B 112 (1982) 173

[6] NA35 Collaboration, A. Bamberger *et al., Phys. Lett.* B 184 (1987) 271

[7] UA1 Collaboration, G. Arnison *et al.,* CERN-EP-82/122, presented to the XXI International Conference on High Energy Physics, Paris, 1982 (unpublished); See also UA1 Collaboration, G. Arnison *et al., Phys. Lett.* B 107 (1981) 320

[8] UA2 Collab., M. Banner *et al., Phys. Lett.* B 118 (1982) 203

[9] J. D. Bjorken, *Phys. Rev.* D 27 (1983) 140

[10] E802 Collaboration, T. Abbott *et al., Phys. Lett.* B 197 (1987) 285 ; E802 Collaboration, L.P. Remsberg, M.J. Tannenbaum *et al., Z. Phys.* C 38 (1988) 35

[11] A. Białas, A. Błeszynski and W. Czyż, *Nucl. Phys.* B 111 (1976) 461

[12] A. Białas, W. Czyż and L. Lesniak, *Phys. Rev.* D 25 (1982) 2328

[13] WA80 Collaboration, S.P. Sorensen *et al., Z. Phys.* C 38 (1988) 3, 51 ; R. Albrecht *et al., Phys. Lett.* B 199 (1987) 297 ; *Phys. Rev.* C 44 (1991) 2736

[14] See also W. Busza, *et al., Phys. Rev.* D 22 (1980) 13

[15] BCMOR Collaboration, A.L.S. Angelis *et al., Phys. Lett.* B 168 (1986) 158 ; *Phys. Lett.* B 141 (1984) 140

[16] T. Ochiai, *Z. Phys.* C 35 (1987) 209 ; *Phys. Lett.* B 206 (1988) 535 , and references therein.

[17] E802 Collaboration, T. Abbott *et al., Phys. Rev.* C 63 (2001) 064602 ; *Phys. Rev.* C 68 (2003) 034908

[18] E802 Collaboration, T. Abbott *et al., Phys. Rev.* C 45 (1992) 2933

[19] M. J. Tannenbaum, *Phys. Lett.* B 498 (2001) 29

[20] PHENIX Collaboration, K. Adcox *et al., Phys. Rev. Lett.* 86 (2001) 3500 ; *Phys. Rev. Lett.* 87 (2001) 052301 ; see also PHENIX Collaboration, A. Bazilevsky, *et al.,* `nucl-ex/0304015`

[21] PHOBOS Collaboration, B. B. Back *et al., Phys. Rev. Lett.* 85 (2000) 3100

[22] PHENIX Collaboration, S. S. Adler *et al.,* `nucl-ex/0310005`

[23] CERES Collaboration, D. Adamova *et al.,* `nucl-ex/0305002`